Stress Monitoring of Prestressed Steel Strand Based on Magnetoelastic Effect under Weak Magnetic Field Considering Material Strain

Lei Liu[1], Senhua Zhang[2, 3], Yinghao Qu[2, 3], Jianting Zhou[2, 3], Feixiong Yang[4], Rong Liu[5], and Leng Liao[2, 3, *]

Abstract—Prestressed steel strands are critical components of prestressed structures, which determine the bearing capacity of the structures. The prestress loss of steel strands causes the bearing capacity to decline. To monitor the stress of prestressed steel strands, a stress monitoring method based on the magnetoelastic effect was proposed. The influence of the material strain was considered to improve monitoring accuracy. To do the monitoring, a coil-based sensor, using a small excitation current to generate a necessary magnetic field, was employed. The sensor converted the stress into inductance. An experimental system was set up, and two batches of specimens were tested. The experimental results showed that the measured inductance was stable and repeatable. There was a nonlinear relationship between the inductance and the stress. Strands of different batches need to be calibrated separately to obtain the inductance-stress equation. Based on the calibration equation and measured inductance, the stress of strands could be calculated. The difference between the calculated stress and the actual stress was small. Besides, to improve the accuracy and ease of the construction, the self-induction coil of the senor should be one layer and with moderate turns.

1. INTRODUCTION

Prestressed concrete structures have the advantages of high safety and reliability, material saving, low dead weight, high crack resistance, and high rigidity [1]. About 75% of prestressed structures use prestressed steel strands as prestressed tendons [2, 3]. As the critical component of prestressed structures, the stress of prestressed steel strands affects the bearing capacity of structures. With the service time increasing, unpredictable prestress loss occurs under the combined effect of load and environment [4, 5]. The prestress loss of the strand causes the bearing capacity of prestressed structures to decline. To know the performance of prestressed structures, the stress monitoring of prestressed steel strands should be done. The stress monitoring also contributes to health monitoring and maintenance of the structure which has important social and economic values.

Many researchers have studied the stress testing and monitoring of prestressed steel strands and proposed destructive and non-destructive testing methods. The representative of destructive testing methods is the stress release method. The stress release method cuts the strand to release structural stress [6]. Although the accuracy of this method is high, the cutting affects the performance of the prestressed steel strand. Nondestructive testing methods include ultrasonic guided wave method [7, 8], stress wave method [9], fiber grating sensor method [10, 11], acoustic emission method [12, 13] and shape

memory alloy method [14]. The ultrasonic guided wave method determines the stress by analyzing the vibration and transmission speed of the elastic wave in the steel strand. For internal prestressed steel strands, the ultrasonic guided wave can hardly penetrate the concrete, which is suitable for small structures. The stress wave method determines the stress by the velocity of the longitudinal stress wave propagating along the prestressed steel strand. The stress wave method is suitable for prestressed steel strands up to 40 m in length, but the signal-to-noise ratio of the stress wave decays quickly. The fiber grating sensor detection method calculates the stress of the steel strand through the change of the wavelength of the light wave. However, the grating sensor is affected by temperature and coupling agents. Acoustic emission and shape memory alloy methods are still at the laboratory stage. Therefore, the stress monitoring of prestressed steel strands needs further research.

The stress monitoring based on the magnetoelastic effect method is mainly used for cables and external prestressing tendons. The magnetoelastic effect method obtains the stress by measuring electromagnetic parameters [15], such as magnetic permeabilities [16], induced magnetic inductances [1], and the signal of magneto-electric sensors [17]. The magnetoelastic effect method has the characteristics of good dynamic response and little environmental impact. Traditional coil-based sensors [16, 18] and elasto-magneto-electric sensors [17] contain an excitation unit and an induction unit [19]. The sensor is large and requires a large excitation current, thus embedding the sensor in structure is difficult and it is unsuitable for stress monitoring of internal prestressing tendons.
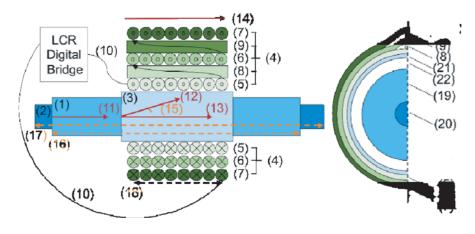
To overcome these bottlenecks, a stress monitoring method based on the magnetoelastic effect under a weak magnetic field considering material strain was proposed. A coil-based sensor, using a small excitation current to generate a necessary magnetic field, was employed to do the monitoring. To verify the feasibility of the proposed monitoring method, a stress monitoring experiment was done. In the experiment, specimens were tested to obtain the stress-inductance relationship. Experimental results demonstrated that the stress-inductance relationship agreed with the theoretical analysis. After the stress-inductance equation (including the free parameters) was obtained by calibration, the stress of strands could be calculated according to the measured inductance. The calculated stress differed little with the actual stress. Then, the influence of sensor parameters on stress monitoring was analyzed. According to the analysis, the sensor design method was proposed. After specified the sensors, the corresponding inductance-stress relationship could be obtained by calibration. Then, the stress of the prestressed steel strand could be ascertained by the inductance of the sensor that is embedded in the structure.

2. STRESS MONITORING PRINCIPLE

The magnetoelastic effect points out the magnetization of ferromagnetic materials changes under stress [20]. Combined with the self-inductance phenomenon, the stress is transformed into an easily measured inductance of the sensor. The main body of the sensor is a coil that acts as the excitation unit and the induction unit of traditional magnetoelastic sensors. As shown in Figure 1, unlike traditional magnetoelastic sensors, the proposed sensor uses a small excitation current to generate the excitation magnetic field. The weak excitation magnetic field is strong enough to magnetize the prestressed steel strand. The strength of the excitation magnetic field is expressed by Equation (1), where H is the strength of the excitation magnetic field, N the turns of the coil, I the small excitation current, and l the length of the magnetic path.

$$H = \frac{NI}{l} \tag{1}$$

The magnetization of the prestressed steel strand could be characterized by its permeability. According to the magnetoelastic effect, the magnetic permeability of the steel strand varied with its stress. Explained by the famous joule theory [21], the relationship between the stress and the magnetization can be expressed as Equation (2). In Equation (2), σ is the stress of the steel strand, E the Young's modulus of the steel strand, λ_s the axial strain constant of the steel strand, M_s the saturation magnetization of the steel strand, K_u the anisotropy constant of the uniaxial magnetization of the steel strand, θ_0 the angle between the easy magnetization axis of the steel strand and the direction of the magnetic field, and ΔM the change in the magnetization of the steel strand. ΔM is determined by the magnetic permeability of the steel strand. The magnetic permeability correlates to the stress.

Figure 1. Schematic diagram of the sensor and steel strand:(1) Steel strand free from stress; (2) Steel strand under stress;(3) Sensor skeleton; (4) Coil that contains (5), (6), (7), (8), and (9); (5) First layer of the coil; (6) Second layer of the coil; (7) Third layer of the coil; (8) Wire from (5) to (6); (9) Wire from (6) to (7); (10) Lead lire of the coil; (11) Axial direction of (1) and (2); (12) Easy magnetization axis of (1) and (2); (13) Direction of the magnetic field; (14) Direction of winding the coil; (15) Angle between (12) and (13); (16) Length of (1); (17) Length of (2); (18) Length of the magnetic path; (19) Sectional Area of (1); (20) Sectional Area of (2); (21) Sectional Area of (3); (22) Sectional Area between (4) and (1) or (2).

Thus, ΔM can be expressed as in Equation (3). In Equation (3), μ_{s0} is the magnetic permeability of the steel strand free from stress, and μ_s is the magnetic permeability of the steel strand at different stress levels.

$$\sigma = E\frac{3\lambda_s M_s}{2K_u}\Delta M \sin^2 \theta_0 cos\theta_0 \tag{2}$$

$$\Delta M = H \cdot (\mu_s - \mu_{s0}) \tag{3}$$

According to the Faraday law of electromagnetic induction and Lenz law, the inductance of the coil relates to the magnetic permeability of the steel strand. The inductance of the coil could be calculated using Equation (4), where A_s is the sectional area of the steel strand, A_0 the area between the coil and the steel strand, and u_0 the magnetic permeability of nonferromagnetic material [22].

$$L = \left(\frac{\mu_s A_s + \mu_0 A_0}{l}\right) N^2 \tag{4}$$

When the excitation current remains constant, there is a functional relationship between inductance and stress as shown in Equation (5), where L_0 is the inductance of the steel strand free from stress.

$$\sigma = E\frac{3\lambda_s M_s}{2K_u}\sin^2 \theta_0 \cos \theta_0 \frac{I}{N \times A_s}(L - L_0) \tag{5}$$

For the specified steel strand and sensor, E, λ_s, M_s, K_u, θ_0, and N are constants, so Equation (5) is rewritten as Equation (6), where W is calculated using Equation (7).

$$\sigma = W\frac{L - L_0}{A_s} \tag{6}$$

$$W = E\frac{3\lambda_s M_s}{2K_u}\sin^2 \theta_0 \cos \theta_0 \frac{I}{N_s} \tag{7}$$

In prestressed structures, the stress of the prestressed steel strand is large, resulting in a large change in the sectional area of steel strand. Thus, considering the influence of the material strain could improve the accuracy of the stress monitoring. To this end, the Ramberge-Osgood constitutive relationship [23] is introduced to describe the strain of the steel strand. When the stress does not exceed the elastic limit of the steel strand, the Ramberge-Osgood relationship can be expressed as Equation (8).

In Equation (8), $\sigma_{0.2}$ is a typical set to the 0.2 percent proof (yield) stress of the steel strand. During the loading and unloading, the volume of the strand remains. Equation (8) could be expressed by the sectional area of the steel strand as Equation (9), where V is the volume of the steel strands. Substituting Equation (9) into Equation (6), the nonlinear relationship between the inductance and the stress can be expressed as Equation (10) and Equation (11), where ΔL is the change in inductance.

$$0 \leq \sigma \leq \sigma_{0.2}, \quad \varepsilon = \frac{\sigma}{E} \tag{8}$$

$$\frac{\frac{V}{A_s} - \frac{V}{A_{s0}}}{\frac{V}{A_{s0}}} = \varepsilon \Rightarrow A_s = \frac{EA_{s0}}{\sigma + E} \tag{9}$$

$$\sigma^2 + \sigma = WEA_s(L - L_0) \tag{10}$$

$$\sigma = \frac{E}{2} + \sqrt{WE\Delta L + \frac{E^2}{4}} \tag{11}$$

Preliminary studies found that obtaining the value of W through calibration is difficult. Thus, Equation (11) is expanded using a Taylor Series into Equation (12). During the expansion, the higher-order quantities after the third order are ignored. In Equation (12), a_1, a_2, and a_3 are constants. After obtaining the constants of Equation (12) by calibration, the stress of the prestressed steel strand can be ascertained by the collected inductance of the embedded sensor.

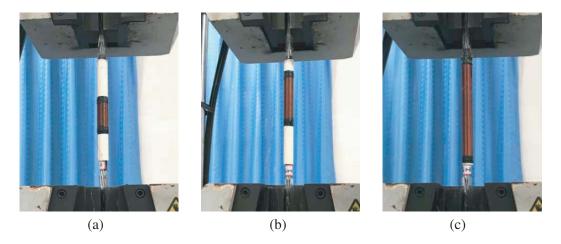$$\sigma = a_1\Delta L^2 + a_2\Delta L + a_3 \tag{12}$$

3. EXPERIMENT DESIGN

To carry out the stress monitoring test of the prestressed steel strand, an experimental system was set up. Nine sensors and twenty-four specimens were prepared. The specimens were tested to verify the proposed stress monitoring method. The influence of the sensor parameters on the stress monitoring was analyzed.

3.1. Sensors and Specimens

To convert the magnetic permeability into inductance, nine sensors, with the main body of self-induction coil, were prepared and labeled according to its parameters. The parameters of the sensors were shown in Table 1. The number of turns of the sensors was 100, 200, and 300, respectively. As shown in Figure 1, to change the length of the magnetic path without changing the number of turns, the number of the winding layers of the sensors was set as 1, 2, and 3, respectively. The purpose of changing the parameters was to investigate its influence on the accuracy of stress monitoring. The coils of the sensors

Table 1. Parameters of the sensors.

Label	Number of turns	Number of layers	Length of the magnetic path /mm
G100-1	100	1	35.0
G100-2	100	2	17.5
G100-3	100	3	11.7
G200-1	200	1	70.0
G200-2	200	2	35.0
G200-3	200	3	23.3
G300-1	300	1	105.0
G300-2	300	2	52.5
G300-3	300	3	35.0

(a)   (b)   (c)

Figure 2. Sensors that were mounted on the specimens: (a) Sensor G100-1; (b) Sensor G200-1; (c) Sensor G300-1.

were composed of 0.35 mm enameled wire, which was wound on a plastic skeleton. The inner diameter of the skeleton was set small to minimize the area between the coil and the steel strand. As shown in Figure 2, after wounding the coil, the sensor was fixed on the steel strand and filled with organic silicone.

The specimens were taken from two batches of steel strands. Six specimens were taken from the first batch of steel strands, and eighteen specimens were taken from the second batch. These two batches of steel strands had the same manufacturers, the same materials, the same production standards, the same production processes, and thus similar properties. The steel strands had a nominal diameter of 15.2 mm, a tensile strength of 1860 MPa, a limit load of 259 kN, and a yield load of 220 kN. The steel strand contained seven steel wires and covered by PE sheath. Each specimen had a length of 0.8 m. To ensure the universal test machine can hold the specimens stably, the sheath with a length of 0.25 m at both ends of the specimens were removed. As shown in Table 2, specimens were tested with different sensors. Two specimens were tested under each working condition to ensure the reliability and repeatability of the test results.

Table 2. Labels and corresponding sensors of specimens.

Label of specimen	The batch of the specimen	Corresponding sensor
G300-1-B1-T1/T2	1	G300-1
G300-2-B1-T1/T2	1	G300-2
G300-3-B1-T1/T2	1	G300-3
G100-1-B2-T1/T2	2	G100-1
G100-2-B2-T1/T2	2	G100-2
G100-3-B2-T1/T2	2	G100-3
G200-1-B2-T1/T2	2	G200-1
G200-2-B2-T1/T2	2	G200-2
G200-3-B2-T1/T2	2	G200-3
G300-1-B2-T1/T2	2	G300-1
G300-2-B2-T1/T2	2	G300-2
G300-3-B2-T1/T2	2	G300-3

3.2. Experiment System

The experiment system was set up to perform stress monitoring. As shown in Figure 3, the system consisted of a universal test machine, clamping pieces, specimens, sensors, an LCR digital bridge, and a computer. The universal test machine, with a maximum tension of 100000 kg, was used to tension the specimen to different stress levels. The aluminum clips wrapped both ends of the specimen. The inner surface of the aluminum clips had quartz sand which increased the friction between the clips and the steel strand. Thus, the universal test machine can hold the specimen more stably.

As shown in Figure 4, the LCR digital bridge connected with the sensor through the 4-wire Kelvin

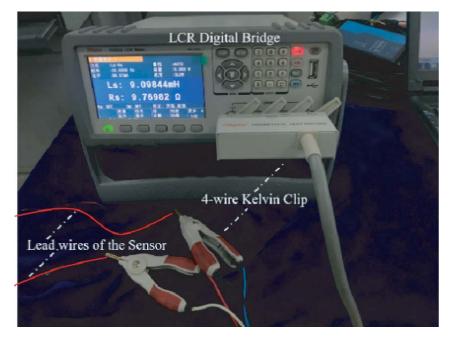
Figure 3. Experimental system and specimens.

Figure 4. The connection between the sensor and the LCR digital bridge.

clip. The LCR digital bridge provided an excitation current to the sensor and collected the inductance of the sensor. The LCR digital bridge provided a sinusoidal AC excitation current with a frequency of 20 Hz and a current intensity of 66.67 mA. Because the inductance of the sensor was small, the inductance was measured in series mode. The internal resistance of the LCR digital bridge was set as 30 Ω. Through the automatic data acquisition software, the inductance measured by the LCR digital bridge was stored in the computer waiting for further processing.

3.3. Loading and Unloading Program

In the experiment, specimens were loaded and then unloaded to simulate the characteristics of the prestressed steel strands. As the prestress of the steel strand using in prestressed structures didn't exceed 75% of its tensile strength, the range of the load was set from 0 kN to 200 kN.

As shown in Figure 5, during the loading phase, the load increased from 0 kN to 200 kN with a step of 10 kN. The loading speed was 0.5 kN/s. At each stress level, the load was maintained for 60 s. To ensure the steel strand was fully deformed and to reduce the error caused by the response lager of the LCR digital bridge, no data was collected during the first 30 s. In the last 30 s, the inductance of the sensor was collected for multiple times. After the loading phase was completed, the specimen was unloaded to 0 kN with the same method.
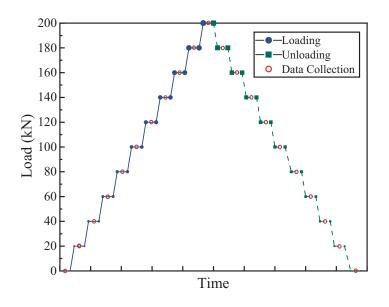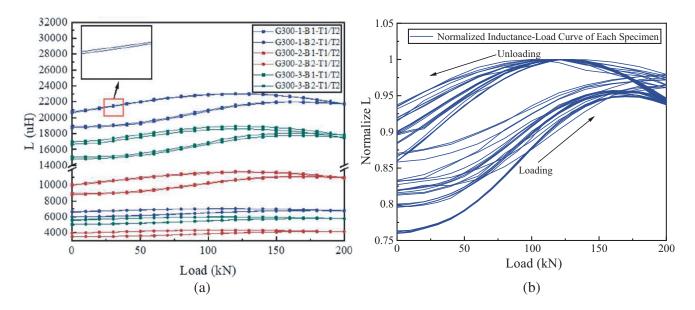

Figure 5. Loading and unloading program.

4. RESULTS AND DISCUSSION

4.1. Relationship between Inductance and Stress

The specimens of two batches were tested, and the results were shown in Figure 6(a). At each load level, the inductance of the sensor was collected for multiple times. The standard deviation of the obtained inductance was small. The small deviation indicated that the inductance was repeatable and stable. The specimens, taken from the same batch and tested with the same sensor, had similar inductance-load curves. Thus, when the sensor was specified, the prestressed steel strands of the same batch had the same inductance-stress curve. After calibrating one or a few prestressed steel strands, the stress of the steel strands can be ascertained using the inductance and the inductance-stress curve. Since the two batches of steel strands were not the same, the physical properties were different, resulting in different inductance-load curves. As shown in Figure 6(a), specimens, taken from different batches but tested with the same sensor, had different inductance-load curves. This meant that different batches of steel strands should be calibrated separately.

Figure 6. Inductance changed with load: (a) Inductance collected at different load levels; (b) Normalized inductance-load curves.

As shown in Figure 6(a), different batches of steel strands and different sensor parameters caused different inductance-load curves. However, the inductance-load relationship of each specimen was consistent. To compare the inductance-load relationship of each specimen, the inductance-load curves of the specimens were normalized. The normalized curves were shown in Figure 6(b). During the loading phase, the inductance increased with the increasing load. During the unloading phase, the inductance increased first and then decreased with the decreasing load. The normalized inductance-load curves of different specimens were similar. Therefore, a representative specimen was selected for further analysis.

Besides, at the same load level, the inductance measured during the loading phase differed with the inductance measured during the unloading phase. Two reasons caused this phenomenon. At first, the prestressed steel strands were hard steel. According to the stress-strain constitutive relationship of the hard steel, the stress-strain relationship in the loading phase and the unloading phase was different. When the specimens were unloaded to 0 kN, residual strain existed. Secondly, the prestressed steel strands were ferromagnetic materials. According to the magneto-mechanical coupling theory, steel strands underwent reversible magnetization and irreversible magnetization when tensioned. The irreversible magnetization of the steel strands still existed after unloading. This irreversible magnetization caused different changes in permeability during the loading phase and the unloading phase. In conclusion, the loading phase and the unloading phase should be discussed separately.

4.2. Stress Monitoring during the Loading Phase

To analyze the stress monitoring of prestressed steel strands during the loading and unloading phases, specimen G300-1-B1-T1 was selected as the representative. The inductance changing with load was shown in Figure 7.

As shown in Figure 7, the inductance-load curve of the loading phase can be divided into three stages. In stage 1, the load increased from 0 kN to 100 kN. As the magnetic permeability of the specimen increased with the load, the measured inductance increased accordingly. The rate of the change of inductance was also increasing. This kind of change was consistent with the magneto-mechanical coupling theory. In stage 2, the load increased from 100 kN to 170 kN. In this stage, the inductance increased with the load, but the increasing rate started to decrease. The decrease in the rate was caused by the strain of the specimen. With the load increased, the sectional area of the specimen decreased and the inductance of the sensor thus decreased. When the reduction of the inductance caused by the strain was close to the increase caused by the load, the increasing rate of the inductance decreased. In
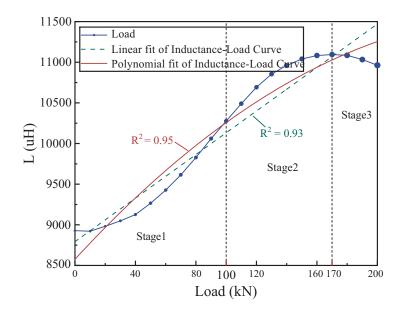
Figure 7. Inductance collected during the loading phase of specimen G300-1-B1-T1.

stage 3, the load increased from 170 kN to 200 kN. At this time, the load was large. The influence of the strain of the specimen on the inductance exceeded the increase caused by the load. Thus, in stage 3, the inductance decreased.

As expressed in Equation (6), when ignoring the influence of material strain, there was a linear relationship between the inductance and the stress. When considered the influence of material strain, there was a nonlinear relationship between the inductance and the stress, as expressed in Equation (12). To verify the necessity of considering the influence of material strain, a linear fit and a nonlinear fit were performed through the least-square method. The fitting results were shown in Figure 8. As shown in Equation (13), the coefficients of determination of the fitting results were calculated to evaluate the fitting. In Equation (13), $y_{real,i}$ is the ith real value of the test index, $y_{fit,i}$ the ith fitted value of the
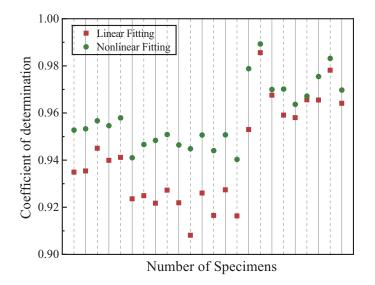

Figure 8. Coefficient of determination of each specimen obtained by linear fit and nonlinear fit during the loading phase.

test index, y_{mean} the mean value of the test index, and R_2 the coefficients of the determination.

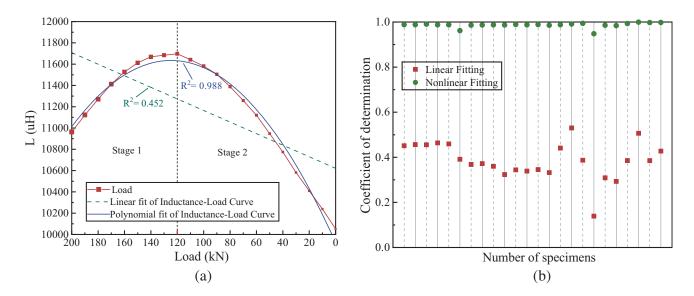$$R^2 = \frac{\sum (y_{fit,i} - y_{mean})^2}{\sum (y_{real,i} - y_{mean})^2} \qquad (13)$$

Ignoring the influence of the material strain, the coefficient of determination of the linear fit was 0.92. The coefficient of determination of the nonlinear fit was 0.95. This result indicated that considering the influence of the material strain could improve the stress monitoring accuracy during the loading phase.

As shown in Figure 8, the coefficient of determination of each specimen was calculated through the linear fit, and the nonlinear fit during the loading phase. The aim was to further analyze the necessity of considering the influence of material strain. Due to the difference between the specimens and the sensors, the determination coefficients of the specimens were different. However, the coefficients obtained by the two methods of each specimen were greater than 0.90. Thus, during the loading phase, the stress can be accurately determined regardless of whether the influence of material strain was considered. In addition, the coefficients of nonlinear fit were greater than the coefficients of the linear fit, which meant considering the material strain improved the accuracy of stress monitoring. Because Equation (6) was simpler and Equation (12) was more accurate, the equations should be chosen according to engineering needs.

4.3. Stress Monitoring during the Unloading Phase

During the unloading phase, the change of the inductance, of specimen G300-1-B1-T1, with the load was shown in Figure 9(a). With the load decreasing, the inductance increased first and then decreased. At the inflection point, the load was 120 kN. The inductance-load curve was thus divided into two stages. The load decreased from 200 kN to 120 kN in stage 1 and decreased from 120 kN to 0 kN in stage 2. In stage 1, with the load decreasing, the sectional area of the specimen increased and the reversible magnetization of the specimen recovered. When the change in the inductance caused by the strain exceeded that caused by the magnetization, the inductance increased as the load decreased. In stage 2, the change in the inductance caused by the strain exceeded that caused by the magnetization, resulting in a decrease in the inductance.

As shown in Figure 9(a), during the unloading phase, the inductance-load curve had strong nonlinearity. The coefficient of determination obtained by linear fit was 0.45, which was much smaller

Figure 9. Analysis of the unloading stage: (a) Inductance collected during the unloading phase of specimen G300-1-B1-T1; (b) Coefficient of determination of each specimen obtained by linear fit and nonlinear fit during the unloading phase.

than that obtained by nonlinear fit, which was 0.99. As shown in Figure 9(b), the coefficient of determination of each specimen was calculated through linear fit and nonlinear fit during the unloading phase. The linear fit and the nonlinear fit were done by using Equation (6) and Equation (12), respectively. The coefficients obtained by the linear fit were less than 0.50, but the coefficients obtained by the nonlinear fit were greater than 0.96. Ignoring the influence of the material strain would cause a great error in stress monitoring. Therefore, to monitor the stress of the prestressed steel strand, the influence of material strain should be considered.

In practical engineering, the prestressed concrete structure has a high density and good integrity. The sensor can be made by winding the coil on the skeleton first, and then pre-buried during the construction of the structure. The same type of prestressed steel strands used in the same structure has similar parameters. Thus, the inductance-stress curve of the steel strands can be obtained by calibration. During the operation of the structure, the inductance measurement device monitors the inductance of the embedded sensor, and then the stress of the prestressed steel strand is calculated. In this way, the prestress monitoring of the prestressed concrete structure is realized.

4.4. Error of Stress Monitoring

When the loading and unloading were finished, the load of the specimens was calculated and compared to the actual load. Before calculated the stress according to Equation (12), a certain specimen of the same batch should be calibrated to obtain the constants in the equation. Since each test condition had two specimens, the specimen labeled T1 was taken as the calibration specimen. The change laws of the inductance with the load during the loading phase and unloading phase were fitted respectively. After obtaining the equation corresponding to different working conditions, the measured inductance was used to calculate the load of the specimens. The calculated load and actual load were shown in Figure 10.
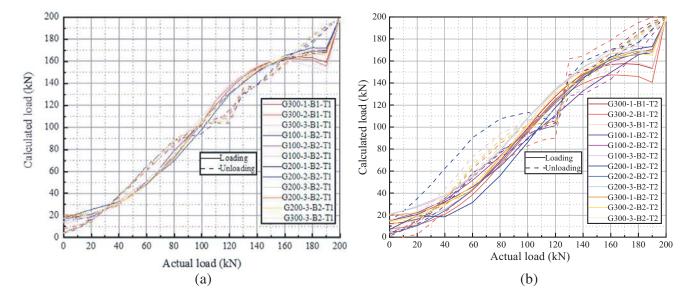

Figure 10. Calculated load and actual load: (a) Load calculated by the inductance of specimen T1 and the equation obtained from specimen T1; (b) Load calculated by the inductance of specimen T2 and the equation obtained from specimen T1.

As shown in Figure 10, comparing the calculated and actual loads, the calculated load was close to the actual load. At most load levels, the relative error did not exceed 10%. Due to the acquisition equipment and environmental factors, the calculated error of specimen labeled T2 was larger than the error of specimen labeled T1. However, the error of stress monitoring was small, which met the engineering requirements. Besides, the error of each specimen of the unloading phase was smaller than the error of the loading phase, which is conducive to monitoring the prestress loss of the steel strand.

4.5. Influence of Sensor Parameters

To optimize the stress monitoring, the influence of the sensor parameters on the stress monitoring was analyzed. In the experiment, the inductance collected by the LCR digital bridge was composed of the true value and measurement error, as shown in Equation (14). In Equation (14), L_a is the actual inductance, L_e the measurement error, and k a constant. Thus, the inductance increment is expressed as Equation (15), where ΔL_a is the increment of L_a, and ΔL_e is the increment of L_e.

$$L = L_a + L_e = \left(\frac{\mu_s A_s + \mu_0 A_0}{l} \right) N^2 + k \left(\frac{\mu_s A_s + \mu_0 A_0}{l} \right) N^2 \tag{14}$$

$$\Delta L = \Delta L_a + \Delta L_e = \Delta L_a + k\Delta L_a \tag{15}$$

Because k related to the collection instrument (LCR digital bridge), for the same instrument, k was a constant. For a certain collection instrument, the inductance of the sensor controlled the value of the measurement error. Combining Equation (12) and Equation (15), the error of the calculated stress was expressed as Equation (16), where σ_{error} is the error of the stress, σ_{cal} the calculated stress, and σ_a the actual value of the stress. When the test instrument was specified, the error of the stress monitoring increased with the increase of the turns of the sensor and decreased with the length of the magnetic path of the sensor.

$$\sigma_{error} = \sigma_{cal} - \sigma_a = \left(a_1(\Delta L_a + k\Delta L_a)^2 + a_2(\Delta L_a + k\Delta L_a) + a_3 \right) - \left(a_1\Delta L_a^2 + a_2\Delta L_a + a_3 \right)$$
$$= a_1 k^2 \Delta L_a^2 + 2k\Delta L_a \tag{16}$$

Since the sensor parameters related to the error of stress monitoring, analyzing the influence quantitatively was necessary. For each specimen, the coefficients of determination during the loading phase and unloading phase were calculated through the nonlinear fit. The average of these two coefficients represented the accuracy of the stress monitoring of each sensor. As shown in Table 3, for sensors with the same number of turns, the monitoring accuracy increased with the length of the magnetic path. For sensors with 200 turns, the length of the magnetic path increased from 23.33 mm to 70.00 mm. The coefficient changed 0.01, which meant the length of the magnetic path had little influence on the monitoring accuracy. Thus, to improve the monitoring accuracy, the magnetic length of the coil should be appropriately increased. Because the change of the length of the magnetic length was realized by changing the number of winding layers, reducing the number of winding layers can increase the length of the magnetic path. Besides, reducing the winding layers also reduced the difficulty of producing and installing the sensor.

Table 3. Sensor parameters and coefficients of determination.

Number of turns	Length of the magnetic path /mm	Coefficient of determination
100	11.67	0.9700
	17.5	0.9741
	23.33	0.9829
200	23.33	0.9741
	35	0.9782
	70	0.9798
300	35	0.9602
	52.5	0.9657
	105	0.9683

For sensors with the same length of magnetic path, the monitoring accuracy decreased with the increase of the number of turns, which agreed with Equation (14) and Equation (16). To improve monitoring accuracy, the number of turns should be reduced. Since the sensor inductance was proportional to the square of the number of turns, a decrease in the number of turns would cause

the inductance to decrease rapidly. When the inductance was too low, the influence of the environment was more significant, which affected the monitoring accuracy. Thus, the length of the magnetic path should be selected reasonably. In the experiment, the best sensor was G200-1. The number of winding layers was one and the number of turns was 200. In engineering applications, to improve the monitoring accuracy and reduce the difficulty of installation, the number of turns should be moderate, and the number of winding layers should be one.

5. CONCLUSION

To monitor the stress of prestressed steel strands, a stress monitoring method based on the magnetoelastic effect was proposed. The main body of the sensor was a self-induction coil which provided a weak magnetic field and converted the stress into inductance. The influence of the material strain is considered to improve monitoring accuracy. Two batches of specimens were tested to verify the feasibility and accuracy of the monitoring method. The main conclusions were drawn as follows.

(1) Different batches of prestressed steel strands had different magnetic characteristics and thus different inductance-stress relationships. To perform stress monitoring, different batches of steel strands should be calibrated separately.

(2) The change law of the inductance with stress was different during the loading and unloading phases. During the loading stage, whether or not the material strain was considered, the stress can be accurately monitored. During the unloading stage, the influence of the material strain should be considered.

(3) Based on the experimental results, the load of each specimen was calculated. The error between the calculated load and actual load was small, which met the engineering needs.

(4) The influence of sensor parameters on the accuracy of steel strand stress monitoring was evaluated. To improve the monitoring accuracy and reduce the difficulty of installation, the number of the coil turns should be moderate, and the number of winding layers should be one.

ACKNOWLEDGMENT

REFERENCES

1. Ahlborn, T. M., C. K. Shield, and C. W. French, "Full-scale testing of prestressed concrete bridge girders," *Experimental Techniques*, Vol. 21, No. 1, 33–35, 1997.

2. Bartoli, I., S. Salamone, R. Phillips, F. Lanza Di Scalea, S. Coccia, and C. S. Sikorsky, "Monitoring prestress level in seven wire prestressing tendons by inter wire ultrasonic wave propagation," *Advances in Science and Technology*, Vol. 56, 200–205, 2008.

3. Bymaster, J. C., C. N. Dang, R. W. Floyd, and W. M. Hale, "Prestress losses in pretensioned concrete beams cast with lightweight self-consolidating concrete," *Structures*, Vol. 2, 50–57, 2015.

4. Cappello, C., D. Zonta, H. A. Laasri, B. Glisic, and M. Wang, "Calibration of elasto-magnetic sensors on in-service cable-stayed bridges for stress monitoring," *Sensors (Basel, Switzerland)*, Vol. 18, No. 2, 466, 2018.

5. Chen, L., J. Chen, and J. Wang, "Calculation of reasonable tension value for longitudinal connecting reinforcement of CRTSII slab ballastless track," *Applied Sciences*, Vol. 8, No. 11, 2139, 2018.

6. Duan, Y., R. Zhang, Y. Zhao, S. Or, K. Fan, and Z. Tang, "Smart Elasto-Magneto-Electric (EME) sensors for stress monitoring of steel structures in railway infrastructures," *Journal of Zhejiang University — SCIENCE A*, Vol. 12, No. 12, 895–901, 2011.

7. Duan, Y., R. Zhang, Y. Zhao, S. Wing Or, K. Fan, and Z. Tang,, "Steel stress monitoring sensor based on elasto-magnetic effect and using magneto-electric laminated composite," *Journal of Applied Physics*, Vol. 111, No. 7, 07E516-07E516-3, 2012.

8. Garcia, T., W. J. Hornof, and M. F. Insana, "On the ultrasonic properties of tendon," *Ultrasound in Medicine & Biology*, Vol. 29, No. 12, 1787–1797, 2003.

9. Jang, J. B., K. M. Hwang, H. P. Lee, and B. H. Kim, "An assessment of the prestress force on the bonded tendon by SI and impact signal analysis techniques," *Nuclear Engineering and Design*, Vol. 255, 9–15, 2013.

10. Jeong, S., W. Jang, J. Nam, H. An, and D. Kim, "Development of a structural monitoring system for cable bridges by using seismic accelerometers," *Applied Sciences*, Vol. 10, No. 2, 716, 2020.

11. Joh, C., J. W. Lee, and I. Kwahk, "Feasibility study of stress measurement in prestressing tendons using villari effect and induced magnetic field," *International Journal of Distributed Sensor Networks*, Vol. 9, No. 11, 249829, 2013.

12. Kim, Y., N. Huh, Y. Kim, Y. Choi, and J. Yang, "On relevant ramberg-osgood fit to engineering nonlinear fracture mechanics analysis," *Journal of Pressure Vessel Technology*, Vol. 126, No. 3, 277–283, 2004.

13. Li, C., J. He, Z. Zhang, Y. Liu, H. Ke, C. Dong, and H. Li, "An improved analytical algorithm on main cable system of suspension bridge," *Applied Sciences*, Vol. 8, No. 8, 1358, 2018.

14. Lv, X. J., X. F. Zhao, L. Wang, H. Dong, and Y. F. Zhu, "Research on fiber Bragg grating sensing technique for cable tension monitoring of suspension bridges," *Applied Mechanics and Materials*, Vol. 368–370, 1391–1395, 2013.

15. Maji, A. K., "Evaluation of prestressing with a shape memory alloy," *MRS Proceedings*, Vol. 503, 1997.

16. Sathyan, S., U. Aydin, A. Lehikoinen, A. Belahcen, T. Vaimann, and J. Kataja, "Influence of magnetic forces and magnetostriction on the vibration behavior of an induction motor," *International Journal of Applied Electromagnetics and Mechanics*, Vol. 59, No. 3, 825–834, 2019.

17. Schoenekess, H. C., "Method to determine tensile stress alterations in prestressing steel strands by means of an Eddy-current technique," *IEEE Sensors Journal*, Vol. 7, No. 8, 1200–1205, 2007.

18. Shu, Y., W. Chen, P. Zhang, J. Wu, L. Liu, and X. Zhao, "Embedding technology of Fiber Bragg Grating strain sensor for cable tension monitor," *Proc. SPIE 9044, 2013 International Conference on Optical Instruments and Technology: Optical Sensors and Applications*, 90440H-90440H-11, 2013.

19. Sumitro, S., A. Jarosevic, and M. L. Wang, "Elasto-magnetic sensor utilization on steel cable stress measurement. Monitoring," *The First Fib Congress, Concrete Structures in the 21th Century*, 2002.

20. Wang, M. L., "Magnetoelastic permeability measurement for stress monitoring in steel tendons and cables," *Proc. SPIE 3995, Nondestructive Evaluation of Highways, Utilities, and Pipelines IV*, Jun. 9, 2000.

21. Tang, D., S. Huang, W. Chen, and J. Jiang, "Study of a steel strand tension sensor with difference single bypass excitation structure based on the magneto-elastic effect," *Smart Mater. Struct.*, Vol. 17, 25019, 2008.

22. Soohoo, R., "Magnetic thin film inductors for integrated circuit applications," *IEEE T. Magn.*, Vol. 15, 1803–1805, 1979.

23. Zagrai, A., V. Gigineishvili, W. A. Kruse, A. Murray, D. Doyle, W. Reynolds, B. Arritt, and H. Gardenier, "Acousto-elastic measurements and baseline-free assessment of bolted joints using guided waves in space structures," *Proceedings of SPIE — The International Society for Optical Engineering*, 765017–7650112, 2010.